Determination of hadron-quark phase transition line from lattice QCD and two-solar-mass neutron star observations

Junpei Sugano,[1,*] Hiroaki Kouno,[2,†] and Masanobu Yahiro[1,‡]

[1]*Department of Physics, Graduate School of Sciences, Kyushu University, Fukuoka 819-0395, Japan*
[2]*Department of Physics, Saga University, Saga 840-8502, Japan*

(Received 12 May 2016; published 20 July 2016)

We aim at drawing the hadron-quark phase transition line in the QCD phase diagram by using the two-phase model (TPM) in which the entanglement Polyakov-loop extended Nambu-Jona-Lasinio (EPNJL) model with the vector-type four-quark interaction is used for the quark phase and the relativistic mean field (RMF) model is used for the hadron phase. A reasonable TPM is constructed by using lattice QCD data and neutron star observations as reliable constraints. For the EPNJL model, we determine the strength of vector-type four-quark interaction at zero quark chemical potential from lattice QCD data on quark number density normalized by its Stefan-Boltzmann limit. For the hadron phase, we consider three RMF models: NL3; TM1; and the model proposed by Maruyama, Tatsumi, Endo, and Chiba (MTEC). We find that MTEC is most consistent with the neutron star observations and TM1 is the second best. Assuming that the hadron-quark phase transition occurs in the core of a neutron star, we explore the density dependence of vector-type four-quark interaction. Particularly for the critical baryon chemical potential $\mu_{\rm B}^{\rm c}$ at zero temperature, we determine a range of $\mu_{\rm B}^{\rm c}$ for the quark phase to occur in the core of a neutron star. The values of $\mu_{\rm B}^{\rm c}$ lie in the range 1560 MeV $\leq \mu_{\rm B}^{\rm c} \leq$ 1910 MeV.

DOI: 10.1103/PhysRevD.94.014024

I. INTRODUCTION

Temperature (T) and baryon chemical potential ($\mu_{\rm B}$) dependence of quantum chromodynamics (QCD) is often described as the QCD phase diagram [1], where $\mu_{\rm B}$ is related to quark chemical potential $\mu_{\rm q}$ as $\mu_{\rm B} = 3\mu_{\rm q}$. Investigation of the truth about the QCD phase diagram is quite important not only in hadron physics but also in astrophysics. Lattice QCD (LQCD) simulation as the first principle calculation is a powerful tool of studying the QCD phase diagram. In fact, recent LQCD simulations provide reliable results in $\mu_{\rm q}/T \lesssim 1$ with sophisticated methods [2–11]. However, these methods are considered not to work well in $\mu_{\rm q}/T \gtrsim 1$ because of the severe sign problem. To understand the QCD phase diagram there, the effective model analyses are done extensively; see, e.g., [12–17]. Among the effective models, the entanglement Polyakov-loop extended Nambu-Jona-Lasinio (EPNJL) model is one of the most useful effective models [18]. The 2-flavor EPNJL model is successful in reproducing LQCD data at zero and imaginary $\mu_{\rm q}/T$, isospin chemical potential, and small real $\mu_{\rm q}/T$ [18,19]. In addition, Ishii *et al.* showed very recently that random-phase-approximation calculations based on the EPNJL model well reproduce T dependence of the meson screening masses calculated by LQCD in both the 2- and 2 + 1-flavor cases [20,21].

In spite of this success, the EPNJL model cannot treat the baryon degrees of freedom explicitly, which is a disadvantage in describing the baryon sector in the QCD phase diagram. Another way of describing all the regions of the QCD phase diagram is the two-phase model (TPM) in which the hadron-quark phase transition is assumed to be the first order and the phase boundary is determined by the Gibbs criterion [22,23]. The TPM allows us to use different models for hadron and quark phases. Various methods were proposed and developed so far to describe the hadron phase; for example, the Brueckner-Hartree-Fock method [24], its relativistic version [25], the variational method [26], and the relativistic mean field (RMF) model [27]. Among them, we use the RMF model in this paper since it is easy to treat and successful in describing the saturation properties of nuclear matter. However, the equation of state (EoS) strongly depends on the choice of parameters and is quite different above the normal nuclear density ρ_0. Observations of neutron stars (NSs) may be a key to solve this problem. Recently, two-solar-mass ($2M_{\rm sun}$) NSs were discovered with high accuracy [28,29], and Steiner *et al.* yielded the best fitting against various observed mass-radius (MR) relations [30]. Because the MR relation is sensitive to the EoS taken, we can judge what version of the RMF model is most reasonable above ρ_0.

In the core of heavy NSs, it is possible that the hadron-quark phase transition takes place. The occurrence of the transition depends on the stiffness of the quark-phase EoS, which is sensitive to the strength $G_{\rm v4}$ of the vector-type four-quark interaction. In our previous work [31], the value

*sugano@phys.kyushu-u.ac.jp
†kounoh@cc.saga-u.ac.jp
‡yahiro@phys.kyushu-u.ac.jp

of G_{v4} at $\mu_q/T = 0$ in the EPNJL model was determined from LQCD data on the quark number density n_q normalized by its Stefan-Boltzmann limit n_{SB}; note that n_q/n_{SB} is μ_q-even and has only weak finite-volume effect. The value of G_{v4} obtained in the $\mu_q/T = 0$ limit is called $G_{v4}(0)$ in the present paper. As for n_q/n_{SB}, new LQCD data on n_q were provided by using the extrapolation from the imaginary μ_q/T region to the real one [11]. Since the numerical errors of the new data are very small compared with the previous one based on the Taylor expansion method at real μ_q/T [4], one can determine the value of $G_{v4}(0)$ more sharply.

If the strength G_{v4} is decreasing with increasing μ_q/T, the possibility that the quark phase exists in the core of a NS becomes higher. However, at present, it is difficult to determine the density dependence of G_v theoretically. Hence, here, we consider an inverse problem. When we assume the existence of the quark phase in the core of a NS, how does the existence constrain the density dependence of the strength of G_{v4}? How much should the critical baryon chemical potential of the hadron-quark phase transition be?

In this paper, we first construct reasonable TPMs by using LQCD data at $\mu_q/T = 0$ as a constraint on quark-phase EoS and NS observations as a constraint on both hadron- and quark-phase EoS. As a quark part of TPM, we consider three types of EPNJL models: (1) the model with no vector-type four-quark interaction; (2) the model with vector-type four-quark interaction in which the strength G_{v4} is assumed to be constant, i.e., $G_{v4} = G_{v4}(0)$; and (3) the model with the vector-type four-quark interaction in which the density-dependent strength $G_{v4}(n_q)$ is introduced. The value of $G_{v4}(0)$ is determined from LQCD data on n_q/n_{SB} in the $\mu_q/T = 0$ limit. The density dependence of $G_{v4}(n_q)$ is discussed by assuming that the quark phase takes place in the core of a NS. As hadron phase models, we take three RMF models, i.e., TM1 [32]; NL3 [33]; and the model proposed by Maruyama, Tatsumi, Endo, and Chiba (MTEC) [34]. We determine which hadron-phase EoS is consistent with $2M_{sun}$ NS observations and the statistically analyzed MR relation by Steiner *et al.* [28–30]. We focus our attention on the $2M_{sun}$ region, since our interest is whether the hadron-quark phase transition takes place or not in the core of NS and this possibility becomes higher for heavy NSs. We will find that the MTEC EoS well reproduces all the data on the MR relation, particularly in the $2M_{sun}$ region. The second best is the TM1 EoS.

We then pick up MTEC and TM1 as hadron-phase EoSs and consider six types of TPMs, as shown in Table I. These are classified with the hadron-phase EoS, that is, the MTEC EoS as a TPMa and the TM1 EoS as a TPMb. For each class, we take the EPNJL of types (1)–(3) for the quark-phase EoS. By using TPMa1–TPMa3 and TPMb1–TPMb3, we calculate the MR relation and draw the hadron-quark phase transition line in the $T - \mu_B$ plane. For TPMa3 and TPMb3, varying n_q dependence of $G_{v4}(n_q)$, we determine the upper bound of the transition line for the quark phase to appear in the core of a NS.

TABLE I. TPMs taken in this paper. The TPMs are combinations of the RMF model (MTEC or TM1) and three EPNJL models of types (1)–(3). See the text for the definitions of RMF and EPNJL models.

Class	Hadron-phase EoS	Quark-phase EoS	Label
TPMa	MTEC	EPNJL of type (1)	TPMa1
		EPNJL of type (2)	TPMa2
		EPNJL of type (3)	TPMa3
TPMb	TM1	EPNJL of type (1)	TPMb1
		EPNJL of type (2)	TPMb2
		EPNJL of type (3)	TPMb3

The paper is organized as follows. In Sec. II, we formulate the EPNJL model and the RMF model. The prescription of the Gibbs criterion is also explained. Section III is devoted to show the numerical results. We first determine the value of $G_{v4}(0)$ by using new LQCD data on n_q/n_{SB} in the $\mu_q/T = 0$ limit. Next, we select the RMF model through the comparison with the data on the MR relation. Finally, we construct the TPMa1–TPMa3 and TPMb1–TPMb3. From these models, we draw the upper and lower bounds of the hadron-quark phase transition line from the condition that the quark phase takes place in the core of a NS. The density dependence of the vector-type four-quark interaction is also discussed.

II. MODEL SETTING

A. QUARK PHASE

The Lagrangian of the EPNJL of type (1) is given by

$$\mathcal{L}_{EPNJL} = \bar{q}(i\gamma^\mu D_\mu - m_0)q - \mathcal{U}(\Phi, \Phi^*) + \tilde{G}_{s4}[(\bar{q}q)^2 + (\bar{q}i\gamma_5\vec{\tau}q)^2] - \tilde{G}_{v4}(0)(\bar{q}\gamma_\mu q)^2, \quad (1)$$

where $q = (u, d)^T$ is u- and d-quark fields, $m_0 = \mathrm{diag}(m_u, m_d)$ denotes a current quark mass matrix, and $\vec{\tau}$ is an isospin matrix. In this paper, we set $m_u = m_d \equiv m_0$. The quark and gluon interact through the covariant derivative $D^\mu = \partial^\mu + iA^\mu$, where $A^\mu = g\delta^\mu_0 A^0_a \lambda_a/2 = -ig\delta^\mu_0 (A_4)_a \lambda_a/2$ with gauge field A^μ_a, Gell-Mann matrix λ_a, and the gauge coupling g. $\tilde{G}_{s4}$ and $\tilde{G}_{v4}(0)$ are the strengths of the scalar- and vector-type four-quark interactions depending on the Polyakov loop Φ and its conjugate Φ^*. We parametrize the Polyakov-loop dependence of these interactions as

$$\tilde{G}_{s4} = G_{s4}(1 - \alpha_1\Phi\Phi^* - \alpha_2(\Phi^3 + \Phi^{*3}))$$
$$\tilde{G}_{v4}(0) = G_{v4}(0)(1 - \alpha_1\Phi\Phi^* - \alpha_2(\Phi^3 + \Phi^{*3}))$$

according to the previous works [18,31].

Eventually, the NJL sector of Eq. (1) has five parameters $(m_0, G_{s4}, G_{v4}(0), \alpha_1, \alpha_2)$. We take $G_{s4} = 5.498\ \mathrm{GeV}^{-2}$ and $\alpha_1 = \alpha_2 = 0.2$ of Ref. [18]. The value of $G_{v4}(0)$ will be determined from LQCD data on n_q/n_{SB} [4,11]. In the LQCD data we use, the corresponding current quark mass m_0 was 130 MeV and it is much heavier than the empirical value ~5 MeV. We also keep $m_0 = 130$ MeV for our EPNJL model analysis to determine the value of $G_{v4}(0)$ from the LQCD data.

In the EPNJL model, only the time component of A_a^μ is treated as a homogeneous and static background field. We define Φ and Φ^* in the Polyakov gauge as

$$\Phi = \frac{1}{3}\mathrm{Tr}_c(L), \qquad \Phi^* = \frac{1}{3}\mathrm{Tr}_c(L^\dagger), \tag{2}$$

where $L = \exp[iA_4/T] = \exp[i\mathrm{diag}(A_4^{11}, A_4^{22}, A_4^{33})/T]$ for the classical variables A_4^{ii} satisfying $A_4^{11} + A_4^{22} + A_4^{33} = 0$. Under the definition Eq. (2), we use the logarithm-type Polyakov potential $\mathcal{U}(\Phi, \Phi^*)$ proposed in Ref. [35],

$$\mathcal{U}(\Phi, \Phi^*) = T^4\left[-\frac{a(T)}{2}\Phi\Phi^* + b(T)\log H(\Phi, \Phi^*)\right], \tag{3}$$

where

$$a(T) = a_0 + \left(\frac{T_0}{T}\right) + a_2\left(\frac{T_0}{T}\right)^2,$$
$$b(T) = b_3\left(\frac{T_0}{T}\right)^3$$
$$H(\Phi, \Phi^*) = 1 - 6\Phi\Phi^* + 4(\Phi^3 + \Phi^{*3}) - 3(\Phi\Phi^*)^2.$$

Usually, the parameter T_0 is 270 MeV so as to reproduce LQCD data in the pure gauge limit [36]. For this value of T_0, however, the EPNJL model yields a larger value of pseudocritical temperature T_{pc} for the deconfinement transition than the full-LQCD prediction 171 MeV at $\mu_q/T = 0$ [37–39]. We then rescale T_0 to 190 MeV. By this rescale, the EPNJL model reproduces $T_{pc} = 171$ MeV. Other parameters (a_0, a_1, a_2, b_3) are summarized in Table II.

Here we comment on the μ_q dependence of the Polyakov potential that is induced by the backreaction of the quark sector to the gluon sector. In Ref. [13], μ_q dependence of the parameter T_0 in the Polyakov potential was estimated with the renormalization group method. Near the $T = 0$ axis of the QCD phase diagram of our interest, however, the effect is negligible because the Polyakov loop is small there [40]. We then assume that T_0 is constant in our analyses on LQCD and NS observational data. When the high μ_q/T and large T region is investigated, the μ_q dependence of T_0 cannot be negligible.

TABLE II. The parameter set in the Polyakov potential proposed in Ref. [35]. All parameters are dimensionless.

a_0	a_1	a_2	b_3
3.51	−2.47	15.2	−1.75

After the mean field approximation to Eq. (1), one can obtain the thermodynamic potential Ω_{EPNJL} (per unit volume) as

$$\Omega_{EPNJL} = U_M + \mathcal{U} - 2\sum_{i=u,d} \times \int \frac{d^3\mathbf{p}}{(2\pi)^3}\left[3E_i + \frac{1}{\beta}\log(1 + 3(\Phi + \Phi^* e^{-\beta(E-\tilde{\mu}_i)}) \times e^{-\beta(E-\tilde{\mu}_i)} + e^{-3\beta(E-\tilde{\mu}_i)}) + \frac{1}{\beta}\log(1 + 3(\Phi^* + \Phi e^{-\beta(E+\tilde{\mu}_i)}) \times e^{-\beta(E+\tilde{\mu}_i)} + e^{-3\beta(E+\tilde{\mu}_i)})\right], \tag{4}$$

where $\beta = 1/T$, $U_M = \tilde{G}_{s4}\sigma^2 - \tilde{G}_{v4}(0)n_q^2$, $E = \sqrt{\mathbf{p}^2 + M^2}$ with the constituent quark mass $M = m_0 - 2\tilde{G}_{s4}\sigma$, and $\tilde{\mu}_i = \mu_i - 2\tilde{G}_{v4}(0)n_q$ for $i =$ u, d. The chiral condensate and the quark number density are defined by $\sigma = \langle\overline{q}q\rangle$, $n_q = \langle q^\dagger q\rangle$. We use the three-dimensional momentum cutoff $\Lambda = 631.5$ MeV to regularize the vacuum term. The variables $X = \sigma, n_q, \Phi, \Phi^*$ are determined with stationary condition $\partial\Omega_{EPNJL}/\partial X = 0$. In this paper, we employ the approximation $\Phi = \Phi^*$ since it is known to be a good approximation [18].

In the EPNJL of type (3), the density-dependent strength $G_{v4}(n_q)$ of the vector-type four-quark interaction is introduced. The strength is assumed to be a Gaussian form of

$$G_{v4}(n_q) = \mathrm{e}^{-b\left(\frac{n_q}{\rho_0}\right)^2} G_{v4}(0), \tag{5}$$

where b is a parameter and ρ_0 is a saturation density. Note that the model with vanishing (constant) vector interaction coupling is obtained when $b \to \infty$ ($b \to 0$). The thermodynamic potential of EPNJL of type (3) can be obtained by the replacement $G_{v4}(0) \to G_{v4}(n_q)$. For all types of the EPNJL model, the quark number density n_q is calculated by the thermodynamic relation

$$n_q = -\frac{\partial\Omega_{EPNJL}}{\partial\mu_q}. \tag{6}$$

The determination of the parameter b will be discussed in Sec. III.

B. RELATIVISTIC MEAN FIELD MODEL

We treat the hadron phase by the RMF model. In the RMF model, the nucleon-nucleon interaction is mediated by scalar (φ), vector (ω), and isovector (ρ) mesons. The Lagrangian of the RMF model is written as

TABLE III. Three parameter sets used in the RMF models. The saturation properties derived from the three parameter sets are also summarized. Shown are the saturation density ρ_0, binding energy E_0, incompressibility K, symmetry energy S_0, and ratio of the effective nucleon mass M_N to nucleon mass m_N.

Parameter	MTEC	TM1	NL3
m_N (MeV)	938	938	939
m_φ (MeV)	400	511.198	508.194
m_ω (MeV)	783	783	782.501
m_ρ (MeV)	769	770	763
g_φ	6.3935	10.0289	10.217
g_ω	8.7207	12.6139	12.868
g_ρ	4.2696	4.6322	4.474
$g_2(\mathrm{fm}^{-1})$	−10.757	−7.2325	−10.431
g_3	−4.0452	0.6183	−28.885
c_3	0	71.3075	0
Saturation property	MTEC	TM1	NL3
$\rho_0(\mathrm{fm}^{-3})$	0.153	0.145	0.148
E_0 (MeV)	−16.3	−16.3	−16.3
K (MeV)	240	281	271
S_0 (MeV)	32.5	36.9	37.4
M_N/m_N	0.78	0.63	0.60

$$\begin{aligned}\mathcal{L}_{\mathrm{RMF}} &= \bar{\psi}(i\gamma^\mu\partial_\mu - m_N - g_\varphi\varphi - g_\omega\gamma^\mu\omega_\mu - g_\rho\gamma^\mu\rho_\mu^a\tau_a)\psi \\ &+ \frac{1}{2}\partial^\mu\varphi\partial_\mu\varphi - \frac{1}{2}m_\varphi^2\varphi^2 - \frac{1}{3}g_2\varphi^3 - \frac{1}{4}g_3\varphi^4 \\ &- \frac{1}{4}\Omega^{\mu\nu}\Omega_{\mu\nu} + \frac{1}{2}m_\omega^2\omega^\mu\omega_\mu + \frac{1}{4}c_3(\omega^\mu\omega_\mu)^2 \\ &- \frac{1}{4}R_a^{\mu\nu}R_{\mu\nu}^a + \frac{1}{2}m_\rho^2\rho_a^\mu\rho_\mu^a, \end{aligned} \tag{7}$$

where ψ is the nucleon (N) field and $\Omega^{\mu\nu}$ ($R_a^{\mu\nu}$) is the field strength of the ω (ρ) meson. Masses of the particles are denoted by $m_N, m_\varphi, m_\omega, m_\rho$; Yukawa-coupling constants of the nucleon with mesons are $g_\varphi, g_\omega, g_\rho$; and self-interactions of φ and ω mesons are g_2, g_3, and c_3. We take three RMF models of TM1 [32], NL3 [33], and MTEC [34]. The parameter sets of the three models are summarized in Table III, together with the saturation properties calculated by the models. The saturation densities ρ_0 are slightly different among the three RMF models, as shown in Table III.

Under the mean field approximation, all the meson fields φ, ω, ρ are replaced by the mean values $\langle\varphi\rangle$, $\langle\omega^0\rangle\delta^{\mu 0}$, $\langle\rho_3^0\rangle\delta^{\mu 0}\delta_{a3}$, respectively. For simplicity, these mean values are denoted by φ, ω, ρ. The mean values are determined by the Euler-Lagrange equations,

$$m_\varphi^2\varphi + g_2\varphi^2 + g_3\varphi^3 = -g_\varphi\rho_s, \tag{8}$$

$$m_\omega^2\omega + c_3\omega^3 = g_\omega\rho_B, \tag{9}$$

$$\rho = \frac{g_\rho}{m_\rho^2}\rho_I, \tag{10}$$

where ρ_s, ρ_B, ρ_I are scalar, baryon-number, and isospin densities.

The thermodynamic potential of the RMF model Ω_{RMF} (per unit volume) is then obtained by

$$\begin{aligned}\Omega_{\mathrm{RMF}} &= U_{\mathrm{meson}} - \frac{2}{\beta}\sum_{i=\mathrm{p,n}}\int\frac{d^3\mathbf{p}}{(2\pi)^3} \\ &\times[\log(1+\mathrm{e}^{-\beta(E-\tilde{\mu}_i)}) + \log(1+\mathrm{e}^{-\beta(E+\tilde{\mu}_i)})], \end{aligned} \tag{11}$$

where $E = \sqrt{\mathbf{p}^2 + M_N^2}$ for the nucleon effective mass $M_N = m_N + g_\varphi\varphi$, and

$$\begin{aligned}U_{\mathrm{meson}} &= \frac{1}{2}m_\varphi^2\varphi^2 + \frac{1}{3}g_2\varphi^3 + \frac{1}{4}g_3\varphi^4 \\ &- \frac{1}{2}m_\omega^2\omega^2 - \frac{1}{4}c_3\omega^4 - \frac{1}{2}m_\rho^2\rho^2 \end{aligned}$$

is the mesonic potential. The effective chemical potentials for the neutron (n) and proton (p) are defined by $\tilde{\mu}_{\mathrm{n,p}} = \mu_{\mathrm{n,p}} - g_\omega\omega \pm g_\rho\rho$.

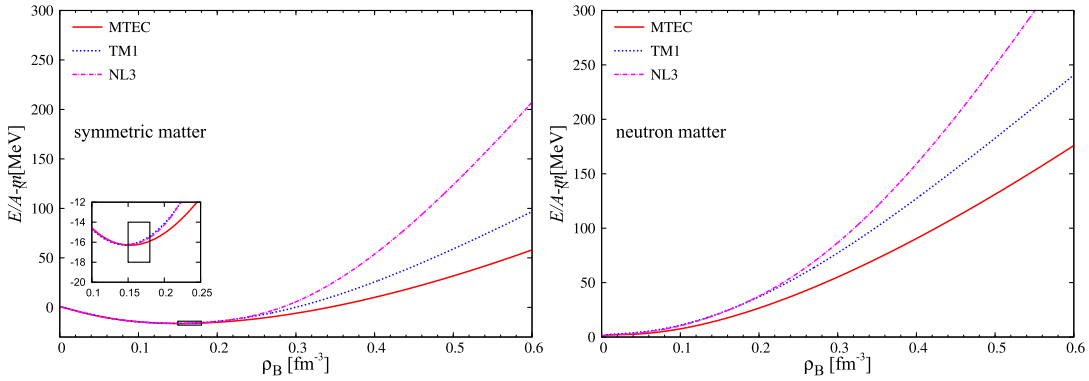

FIG. 1. Equations of state of three parameter sets for symmetric matter (left panel) and neutron matter (right panel). In both panels, the results of MTEC, TM1, and NL3 correspond to the solid, dotted, and dotted-dashed lines, respectively. In the left panel, the open square indicates the empirical saturation point [24].

Figure 1 shows the EoSs of symmetric matter (left panel) and neutron matter (right panel) calculated by TM1, NL3, and MTEC at $T = 0$. As for densities smaller than the saturation point (open square), all the EoSs yield a universal line. On the other hand, there are remarkable differences among the EoSs for densities higher than the saturation point. The MTEC EoS is softest, whereas the NL3 EoS is stiffest. The TM1 EoS lies halfway between them. The behavior of the EoS in $\rho_B \gtrsim \rho_0$ largely affects the MR relation of NSs. Therefore, we can select which EoS model is preferable for the MR relation, particularly in the $2M_{\rm sun}$ region.

C. TWO-PHASE MODEL

In $\mu_{\rm q}/T = 0$, it is established by LQCD simulations that the hadron-quark deconfinement transition is crossover [41]. However, the pseudocritical temperature is well estimated by the TPM [22]. We thus use the TPM and the Gibbs criterion to determine the phase boundary of the hadron-quark phase transition for each set of T and $\mu_{\rm B}$.

Pressures of the EPNJL and the RMF models are obtained by

$$P_{\rm EPNJL}(\mu_{\rm B}, T) = -(\Omega_{\rm EPNJL}(\mu_{\rm B}, T) - \Omega_{\rm EPNJL}(0,0)) - B, \tag{12}$$

$$P_{\rm RMF}(\mu_{\rm B}, T) = -\Omega_{\rm RMF}(\mu_{\rm B}, T), \tag{13}$$

where the bag constant B is introduced in $P_{\rm EPNJL}$ to describe the difference of vacua between the hadron and quark phases. The value of B is so determined that the TPM can reproduce the deconfinement-transition temperature $T_{\rm pc} = 171$ MeV at $\mu_{\rm q}/T = 0$.

According to the Gibbs criterion, the quark phase (hadron phase) takes place when $P_{\rm EPNJL} > P_{\rm RMF}$ ($P_{\rm EPNJL} < P_{\rm RMF}$). Our TPM reproduces $T_{\rm pc} = 171$ MeV, when $B = 100$ MeV^4. We then take $B = 100$ MeV^4 in our analyses.

III. RESULTS

We show our numerical results in this section. We first determine the value of $G_{\rm v4}(0)$ from LQCD data on $n_{\rm q}/n_{\rm SB}$ in the $\mu_{\rm q}/T = 0$ limit [4,11]. As for the RMF model, it is shown that MTEC and TM1 are proper EoSs, through the comparison with NS observations.

Next, from the combinations of the two hadron-phase EoSs and EPNJL types (1)–(3), we construct TPMa1–TPMa3, TPMb1–TPMb3. In the TPMa3 and TPMb3, the density-dependent strength $G_{\rm v4}(n_{\rm q})$ of the vector-type four-quark interaction is introduced. We parametrize the density dependence with a Gaussian form having a single parameter b, shown in Eq. (5). We determine the lower bound of b assuming that the hadron-quark phase transition takes place in the core of a NS. By using six models, the MR relation and the band of the hadron-quark phase transition line that allows the quark phase to exist in the core of NS are calculated.

A. DETERMINATION OF THE VALUE OF $G_{\rm v4}(0)$

In the $T > T_{\rm pc}$ region, the chiral condensate σ is nearly equal to zero, that is, the chiral symmetry is restored. Hence, the scalar-type four-quark interaction becomes negligible and only the vector-type four-quark interaction contributes to the ratio $n_{\rm q}/n_{\rm SB}$ that is $\mu_{\rm q}$-even and therefore finite even in the $\mu_{\rm q}/T = 0$ limit. Thus, we determine the value $G_{\rm v4}(0)$ from LQCD data on $n_{\rm q}/n_{\rm SB}$ at $T > T_{\rm pc}$.

Figure 2 shows T dependence of $n_{\rm q}/n_{\rm SB}$. Here, T is normalized by $T_{\rm pc} = 171$ MeV. In EPNJL model calculations, m_0 is taken to be 130 MeV, as already mentioned in Sec. II. If the vector-type four-quark interaction is zero, the EPNJL model largely overestimates the LQCD data. Meanwhile, good agreement is seen for the case of $G_{\rm v4}(0) = 0.36 G_{\rm s4}$ at high T such as $T = 2T_{\rm pc}$. The comparison between the solid and dashed lines suggests that the entanglement coupling in $G_{\rm v4}(0)$ is necessary to reproduce the LQCD data. The result of $m_0 = 5.5$ MeV is also plotted. Comparing the dotted line with the solid line, we find that m_0 dependence is small at high T. This means that the value of $G_{\rm v4}(0)$ can be determined at high T even if m_0 is heavier than the physical value. For this reason, we use the $G_{\rm v4}(0) = 0.36 G_{\rm s4}$ and set $m_0 = 5.5$ MeV when we analyze the NS property.

B. SELECTION OF RMF MODEL

Now, we select preferable RMF EoSs from the MR relation. The MR relation has one-to-one correspondence to the EoS through the Tolman-Oppenheimer-Volkov (TOV) equation [42]

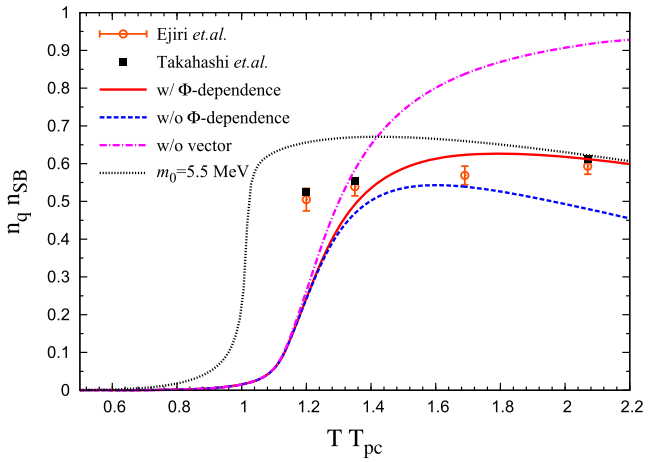

FIG. 2. Temperature dependence of $n_{\rm q}/n_{\rm SB}$ in the $\mu_{\rm q}/T = 0$ limit. The temperature is normalized by the $T_{\rm pc} = 171$ [MeV]. The data are the LQCD results [4,11]. The lines are the results of calculations for the cases with $\tilde{G}_{\rm v4}(0)$ (solid), $G_{\rm v4}(0)$ (dashed), and without the vector-type four-quark interaction (dotted-dashed). The dotted line corresponds to the results with $m_0 = 5.5$ MeV.

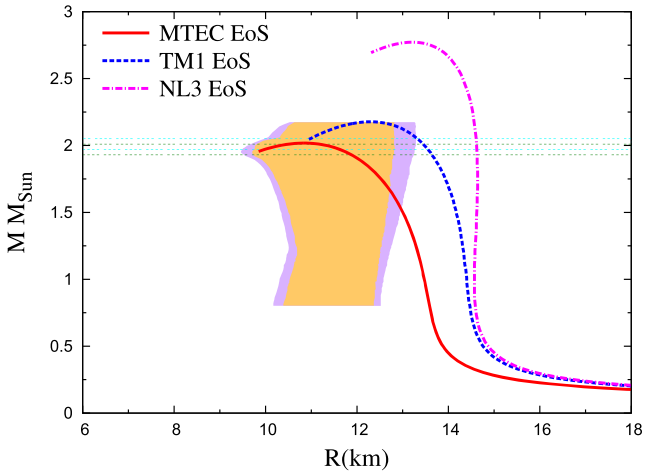

FIG. 3. MR relation for three RMF EoSs. The two horizontal boxes are the $2M_{\rm sun}$ observational data [28,29]. The two areas correspond to the 68% and 95% confidence counters estimated by Steiner *et al.* [30].

$$\frac{dP}{dr} = -G\frac{M\epsilon}{r^2}\left(1+\frac{P}{\epsilon}\right)\left(1+\frac{4\pi Pr^3}{M}\right)\left(1-\frac{2GM}{r}\right)^{-1},$$
$$\frac{dM}{dr} = 4\pi r^2\epsilon,$$

where G is a gravitational constant and ϵ is an energy density. The NS has a crust region at low densities. As an EoS of the crust region, we use that of Miyatsu *et al.* [43].

In solving the TOV equation, the electron and the muon should be taken into account to satisfy the charge neutral condition. We treat the electron as a massless free fermion and the muon as a massive free fermion. If the number densities, $n_{\rm e}$ and n_{μ^-}, of the electron and muon are known, the charge neutral condition is given by

$$n_{\rm p} = n_{\rm e} + n_{\mu^-} \tag{14}$$

for the proton number density $n_{\rm p}$. In the core of a NS, the β-equilibrium condition is also satisfied:

$$\mu_i = b_i\mu_{\rm B} - q_i\mu_{\rm e} \tag{15}$$

for $i = {\rm p, n, e}, \mu^-$, where b_i (q_i) is the baryon number (the electric charge) of particle i and $\mu_{\rm e}$ is the electron chemical potential. Solving the TOV equation numerically with the EoS that satisfies Eqs. (9) and (10), we can get the MR relation.

Figure 3 illustrates the MR relation calculated by the MTEC EoS, TM1 EoS, and NL3 EoS. The data on the MR relation in Fig. 3 are taken from Refs. [28–30]. The maximum mass $M_{\rm max}$ and radius $R_{\rm max}$ are tabulated in Table IV. From Fig. 3, one can see that the MTEC EoS is most consistent with all the data, particularly in the $2M_{\rm sun}$ region. The TM1 EoS predicts a bit larger maximum radius,

TABLE IV. The maximum mass ($M_{\rm max}$) and radius ($R_{\rm max}$) predicted from three RMF models. The mass is normalized by the mass of sun $M_{\rm sun}$.

	MTEC	TM1	NL3
$M_{\rm max}/M_{\rm sun}$	2.02	2.18	2.77
$R_{\rm max}$ (km)	10.8	12.3	13.2

but it reproduces the data of the MR relation considerably well. In the NL3 EoS, the resulting $M_{\rm max}$ and $R_{\rm max}$ are inconsistent with the data of the MR relation. We therefore take the MTEC and TM1 EoSs as the hadron-phase EoS and construct the TPMa1–TPMa3, TPMb1–TPMb3.

C. TRANSITION LINE OF TPMa1 AND TPMb1

We first consider the possibility of the hadron-quark phase transition in the core of NS by using TPMa1 and TPMb1. If the quark phase appears in the core of a NS, the charge neutral and the β-equilibrium conditions should also be imposed on the quark-phase EoS:

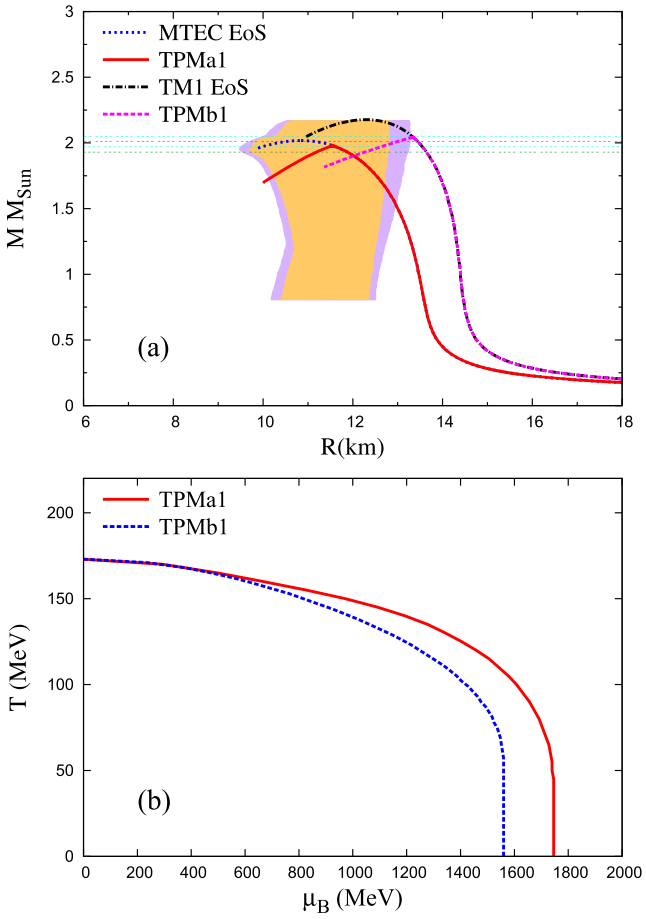

FIG. 4. (a) MR relation calculated from the TPMa1 (solid), TPMb1 (dashed). For comparison, the MR relation calculated from the MTEC and TM1 EoSs are also plotted. (b) Hadron-quark phase transition lines for TPMa1 and TPMb1.

$$\frac{2}{3}n_{\rm u}-\frac{1}{3}n_{\rm d}=n_{\rm e}+n_{\mu^-},$$
$$\mu_{\rm u}=\frac{1}{3}\mu_{\rm B}-\frac{2}{3}\mu_{\rm e},$$
$$\mu_{\rm d}=\frac{1}{3}\mu_{\rm B}+\frac{1}{3}\mu_{\rm e},$$

where $n_{\rm u}$ ($n_{\rm d}$) is the u-quark (d-quark) number density. Which phase is realized is determined from the Gibbs criterion.

In Fig. 4, panel (a) shows the MR relations calculated with TPMa1 and TPMb1. For comparison, the results calculated from the MTEC and TM1 EoSs are plotted. In TPMa1, the quark phase appears at $M=1.97M_{\rm sun}$ before reaching $M_{\rm max}=2.02M_{\rm sun}$ and is consistent with the data on the MR relation. Also in the TPMb1, the quark phase emerges at $M=2.04M_{\rm sun}$ before reaching $M_{\rm max}=2.17M_{\rm sun}$.

Panel (b) of Fig. 4 shows the hadron-quark phase transition line in the $T-\mu_{\rm B}$ plane for TPMa1 and TPMb1. The critical baryon chemical potential $\mu_{\rm B}^{\rm c}$ of the transition at $T=0$ is 1750 MeV for TPMa1 and 1560 MeV for TPMb1. If the $G_{\rm v4}(0)$ is positive, the quark-matter EoS becomes stiffer and thereby the predicted values of the NS mass and $\mu_{\rm B}^{\rm c}$ are increasing. Therefore, TPMa1 and TPMb1 yield the lower bound of $\mu_{\rm B}^{\rm c}$ for each class of TPM for the quark phase to take place in the core of a NS.

D. TRANSITION LINE OF TPMa2 AND TPMb2

Next, we consider TPMa2 and TPMb2 with $G_{\rm v4}(0)=0.36G_{\rm s4}$. Figure 5 illustrates the hadron-quark phase transition line for TPMa1 and TPMa2. One can see that the existence of $G_{\rm v4}(0)$ delays the transition toward higher $\mu_{\rm B}$. The value of $\mu_{\rm B}^{\rm c}$ for TPMa2 is 2600 MeV and the corresponding density is $13\rho_0$. Such a density does not realize in the core of NS and hence the quark phase does not appear in the core of NS for TPMa2.

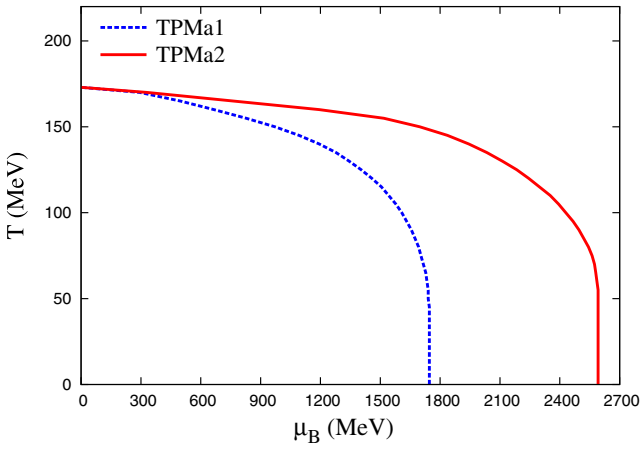

FIG. 5. Hadron-quark phase transition line for TPMa1 and TPMa2.

As for TPMb2, we find that the hadron-quark phase transition line does not reach the $\mu_{\rm B}$ axis. The reason is that the self-interaction $(\omega^\mu\omega_\mu)^2$ of the ω meson further stabilizes the hadron phase with respect to increasing $\mu_{\rm B}$, while the vector-type four-quark interaction suppresses the appearance of the quark phase. In fact, the quark phase is confirmed to never appear in the core of a NS for TPMb2.

E. DENSITY DEPENDENCE OF $G_{\rm v4}$ AND TRANSITION LINE OF TPMa3 AND TPMb3

Finally, we consider TPMa3 and TPMb3. In TPMa3 and TPMb3, the quark phase is described by the EPNJL of type (3); that is, the strength of the vector-type four-quark interaction depends on the quark number density $n_{\rm q}$ [see Eq. (5)]. For TPMa3 (TPMb3), $\rho_0=0.153(0.145)$ fm^{-3} is applied, which is the value predicted by the hadron phase model. The form of Eq. (5) ensures that the interaction is invariant under the charge conjugation and $G_{\rm v4}(n_{\rm q})$ is positive for any $n_{\rm q}$. When $G_{\rm v4}(n_{\rm q})$ is negative, there is the possibility that the vector meson masses calculated with the random-phase approximation become negative. Consequently, the $G_{\rm v4}(n_{\rm q})$ varies in a range $0\le G_{\rm v4}(n_{\rm q})\le G_{\rm v4}(0)=0.36G_{\rm s4}$.

Now, we discuss the lower bound of b by assuming that the quark phase takes place in the core of NS. The left panel of Fig. 6 shows the MR relation calculated with TPMa3. In TPMa3, the quark phase appears at $M_{\rm max}=2.02M_{\rm sun}$ and $n_{\rm q}=7.2\rho_0$, when the value of $G_{\rm v4}(n_{\rm q})$ is equal to $0.12G_{\rm s4}$. This means that $0.12G_{\rm s4}$ is the maximum value of $G_{\rm v4}(n_{\rm q})$ for the quark phase to appear in the core of a NS. The corresponding value of b is 0.001. The right panel of Fig. 6 illustrates the hadron-quark phase transition line. The lower bound of the line is determined by the TPMa1 and the upper bound is the TPMa3 with $b=0.001$. The values of $\mu_{\rm B}^{\rm c}$ lie in the range 1750 MeV $\le\mu_{\rm B}^{\rm c}\le$ 1910 MeV. If the value of $\mu_{\rm B}^{\rm c}$ exists in this region, the hadron-quark phase transition occurs in the core of a NS. Note that the maximum value $\mu_{\rm B}^{\rm c}=1910$ MeV is much smaller than $\mu_{\rm B}^{\rm c}=2600$ MeV in TPMa2 shown in Fig. 5.

The left panel of Fig. 7 shows the MR relation calculated with TPMb3. As for TPMb3, the quark phase appears at $M_{\rm max}=2.17M_{\rm sun}$ and $n_{\rm q}=6\rho_0$, when the value of $G_{\rm v4}(n_{\rm q})$ is equal to $0.18G_{\rm s4}$, which is the maximum value of $G_{\rm v4}(n_{\rm q})$ for the quark phase to appear in the core of a NS in TPMb3. The corresponding value of b is 0.001 and this is common to both TPMa3 and TPMb3. The right panel of Fig. 7 illustrates the hadron-quark phase transition line. The lower bound of the line is determined by the TPMb1 and the upper bound is the TPMb3 with $b=0.001$. The values of $\mu_{\rm B}^{\rm c}$ lie in the range 1560 MeV $\le\mu_{\rm B}^{\rm c}\le$ 1860 MeV. The lower bounds of $\mu_{\rm B}^{\rm c}$ are not the same for TPMa1 and TPMb1, but the upper values for TPMa3 and TPMb3 are nearly equal.

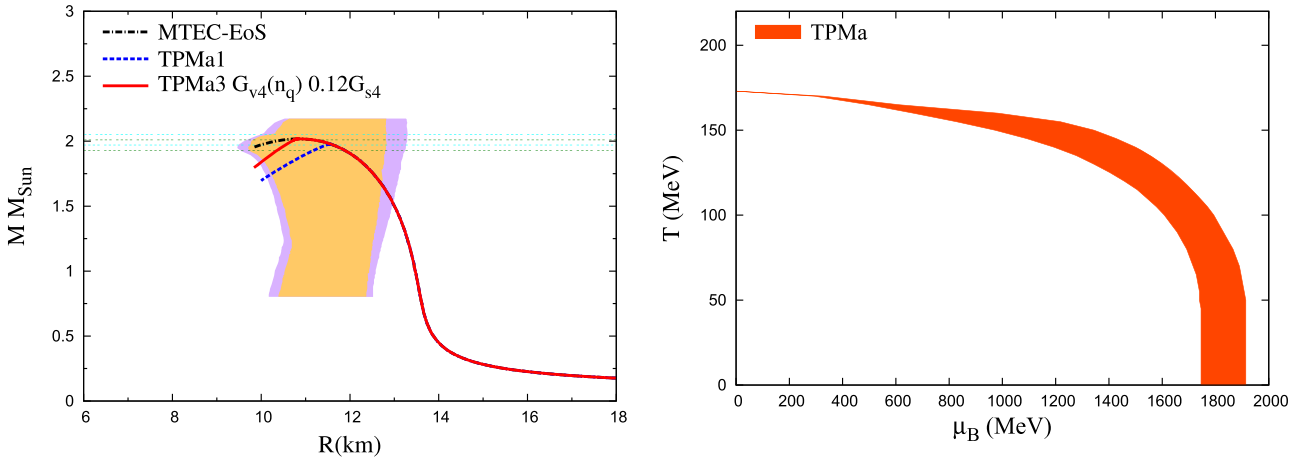

FIG. 6. Left panel: MR relation calculated from TPMa3. The results from the TPMa1 and MTEC EoSs are also plotted. Right panel: Band of the hadron-quark phase transition line. The upper (lower) bound of the band is calculated from TPMa3 (TPMa1). This region allows the quark phase to appear in the core of a NS.

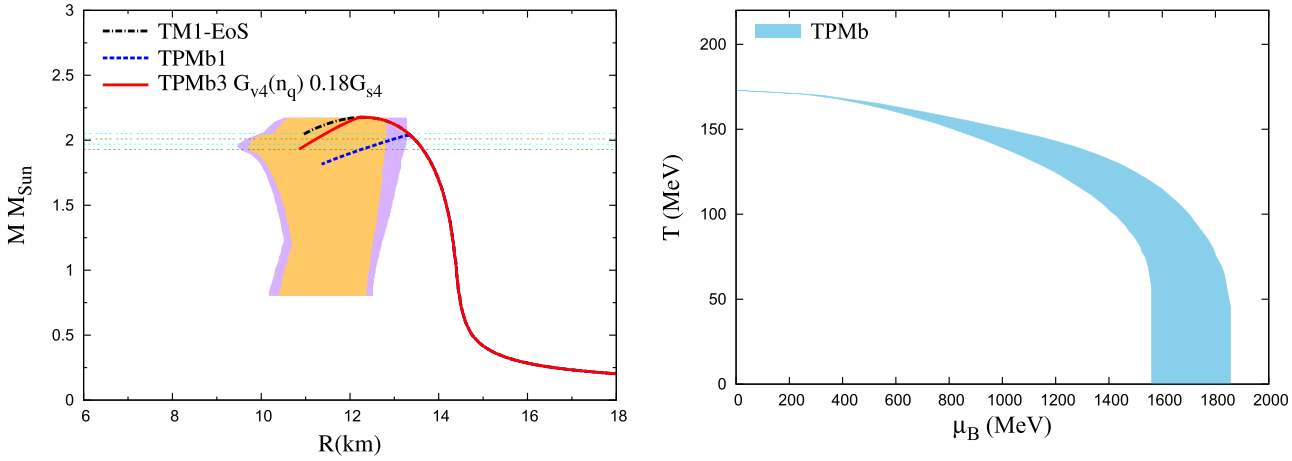

FIG. 7. Left panel: MR relation calculated from TPMb3. The results from the TPMb1 and TM1 EoSs are also plotted. Right panel: Band of the hadron-quark phase transition line. The upper (lower) bound of the band is calculated from TPMb3 (TPMb1). This region allows the quark phase to appear in the core of a NS.

IV. SUMMARY

Understanding of the QCD phase diagram in the whole region of the $\mu_q - T$ plane is a goal of hadron physics. In addition, the diagram on the $T = 0$ axis yields important information on astrophysics. In particular, the location of the hadron-quark phase-transition point on the $T = 0$ axis determines whether the phase transition really occurs in the core of a NS. The sign problem prevents LQCD simulations from approaching the high μ_q/T region. Therefore, the effective model approach is quite essential to explore the appearance of the quark phase in the core of a NS.

In this paper, we constructed the TPM in which the EPNJL model is used in the quark phase and the RMF model is used in the hadron phase. To make the TPM reasonable, we took LQCD data and NS observations as reliable constraints. For the quark-phase model, we determined the density-independent strength $G_{v4}(0)$ of the vector-type four-quark interaction from LQCD data on n_q/n_{SB} in the $\mu_q/T = 0$ limit with small error bars. The obtained value is $G_{v4}(0) = 0.36G_{s4}$, which is a bit larger than that in our previous work. For the hadron phase, we take three RMF models: NL3, TM1 and MTEC. We compared calculated MR relations with observed ones. We found that MTEC is most consistent with the data and TM1 is the second best, while NL3 is inconsistent.

We then take MTEC and TM1 for the hadron part of TPM and considered six types of TPMs (TPMa1–a3 and TPMb1–b3) that are combinations of the two types of hadron-phase EoSs and the EPNJL of types (1)–(3). For TPMa3 and TPMb3, we introduced the density-dependent strength $G_{v4}(n_q)$ of the vector-type four-quark interaction and assumed that the density dependence is described as a Gaussian form having the single parameter b.

The MR relation and hadron-quark phase transition line are calculated for six TPMs. As a result, the hadron-quark phase transition occurs in the core of a NS when 1750 MeV $\leq \mu_B^c \leq$ 1910 MeV for TPMa and 1560 MeV $\leq \mu_B^c \leq$ 1850 MeV for TPMb. For both TPMa and TPMb, the corresponding minimum value of b is $b = 0.001$.

ACKNOWLEDGMENTS

We thank G. M. Mathews, T. Kajino, J. Takahashi, and M. Ishii for useful discussions. J. S., H. K., and M. Y. are supported by Grants-in-Aid for Scientific Research (Grants No. 27-7804, No. 26400279, and No. 26400278) from the Japan Society for the Promotion of Science (JSPS).

[1] K. Fukushima and T. Hatsuda, Rep. Prog. Phys. **74**, 014001 (2011).
[2] Z. Fodor and S. D. Katz, Phys. Lett. B **534**, 87 (2002).
[3] C. R. Allton, S. Ejiri, S. J. Hands, O. Kaczmarek, F. Karsch, E. Laermann, Ch. Schmidt, and L. Scorzato, Phys. Rev. D **66**, 074507 (2002).
[4] S. Ejiri, Y. Maezawa, N. Ukita, S. Aoki, T. Hatsuda, N. Ishii, K. Kanaya, and T. Umeda, Phys. Rev. D **82**, 014508 (2010).
[5] P. de Forcrand and O. Philipsen, Nucl. Phys. **B642**, 290 (2002).
[6] M. D'Elia and M. P. Lombardo, Phys. Rev. D **67**, 014505 (2003).
[7] M. D'Elia and F. Sanfilippo, Phys. Rev. D **80**, 111501 (2009).
[8] L. K. Wu, X. Q. Luo, and H. S. Chen, Phys. Rev. D **76**, 034505 (2007).
[9] P. de Forcrand and O. Philipsen, Phys. Rev. Lett. **105**, 152001 (2010).
[10] J. Takahashi, K. Nagata, T. Saito, A. Nakamura, T. Sasaki, H. Kouno, and M. Yahiro, Phys. Rev. D **88**, 114504 (2013).
[11] J. Takahashi, H. Kouno, and M. Yahiro, Phys. Rev. D **91**, 014501 (2015).
[12] M. Di Toro, A. Drago, T. Gaitanos, V. Greco, and A. Lavagno, Nucl. Phys. **A775**, 102 (2006).
[13] B.-J. Schaefer, J. M. Pawlowski, and J. Wambach, Phys. Rev. D **76**, 074023 (2007).
[14] H. Abuki, R. Anglani, R. Gatto, G. Nardulli, and M. Ruggieri, Phys. Rev. D **78**, 034034 (2008).
[15] M. Ciminale, R. Gatto, N. D. Ippolito, G. Nardulli, and M. Ruggieri, Phys. Rev. D **77**, 054023 (2008).
[16] G. Y. Shao, M. Di Toro, V. Greco, M. Colonna, S. Plumari, B. Liu, and Y. X. Liu, Phys. Rev. D **84**, 034028 (2011).
[17] M. Hempel, V. Dexheimer, S. Schramm, and I. Iosilevskiy, Phys. Rev. C **88**, 014906 (2013).
[18] Y. Sakai, T. Sasaki, H. Kouno, and M. Yahiro, Phys. Rev. D **82**, 076003 (2010).
[19] Y. Sakai, T. Sasaki, H. Kouno, and M. Yahiro, J. Phys. G **39**, 035004 (2012).
[20] M. Ishii, T. Sasaki, K. Kashiwa, H. Kouno, and M. Yahiro, Phys. Rev. D **89**, 071901(R) (2014).
[21] M. Ishii, K. Yonemura, J. Takahashi, H. Kouno, and M. Yahiro, Phys. Rev. D **93**, 016002 (2016).
[22] T. Sasaki, N. Yasutake, M. Kohno, H. Kouno, and M. Yahiro, arXiv:1307.0681.
[23] O. Lourenco, M. Dutra, A. Delfino, and M. Malheiro, Phys. Rev. D **84**, 125034 (2011).
[24] M. Kohno, Prog. Theor. Exp. Phys. **2015**, 123D02 (2015).
[25] R. Brockmann and R. Machleidt, Phys. Rev. C **42**, 1965 (1990).
[26] A. Akmal, V. R. Pandharipande, and D. G. Ravenhall, Phys. Rev. C **58**, 1804 (1998).
[27] B. D. Serot and J. D. Walecka, Adv. Nucl. Phys. **16**, 1 (1986).
[28] P. B. Demorest, T. Pennucci, S. M. Ransom, M. S. E. Roberts, and J. W. T. Hessels, Nature (London) **467**, 1081 (2010).
[29] J. Antoniadis *et al.*, Science **340**, 1233232 (2013).
[30] A. W. Steiner, J. M. Lattimer, and E. F. Brown, Astrophys. J. **722**, 33 (2010).
[31] J. Sugano, J. Takahashi, M. Ishii, H. Kouno, and M. Yahiro, Phys. Rev. D **90**, 037901 (2014).
[32] K. Sumiyoshi, H. Kuwahara, and H. Toki, Nucl. Phys. **A581**, 725 (1995).
[33] G. A. Lalazissis, J. König, and P. Ring, Phys. Rev. C **55**, 540 (1997).
[34] T. Maruyama, T. Tatsumi, T. Endo, and S. Chiba, arXiv: quant-ph/0605075.
[35] S. Rößner, C. Ratti, and W. Weise, Phys. Rev. D **75**, 034007 (2007).
[36] G. Boyd, J. Engels, F. Karsch, E. Laermann, C. Legeland, M. Lütgemeier, and B. Petersson, Nucl. Phys. **469**, 419 (1996).
[37] W. Söldner, *Proc. Sci.*, LAT2010 (2010) 215.
[38] K. Kanaya, AIP Conf. Proc. **1343**, 57 (2011); *Proc. Sci.*, LAT2010 (2010) 012.
[39] S. Borsányi, Z. Fodor, C. Hoelbling, S. D. Katz, S. Kreig, C. Ratti, and K. K. Szabo, J. High Energy Phys. 09 (2010) 073.
[40] T. Sasaki, Y. Sakai, H. Kouno, and M. Yahiro, Phys. Rev. D **82**, 116004 (2010).
[41] Y. Aoki, G. Endrődi, Z. Fodor, S. D. Katz, and K. K. Szabó, Nature (London) **443**, 675 (2006).
[42] S. L. Shapiro and S. A. Teukolsky, *Black Holes, White Dwarfs and Neutron Stars* (Wiley, New York, 1983).
[43] T. Miyatsu, S. Yamamuro, and K. Nakazato, Astrophys. J. **777**, 4 (2013).